Coordination Polymers Based on a Glycine-Derivative Ligand

Sérgio M. F. Vilela,[a,b] Duarte Ananias,[a] Patrícia Silva,[a] Mariela Nolasco,[a] Luís D. Carlos,[c] Verónica de Zea Bermudez,[d] João Rocha,[a] João P. C. Tomé,[b] Filipe A. Almeida Paz[a,*]

A contribution from

[a] *Department of Chemistry, CICECO, University of Aveiro, 3810-193 Aveiro, Portugal*

[b] *Department of Chemistry, QOPNA, University of Aveiro, 3810-193 Aveiro, Portugal*

[c] *Department of Physics, CICECO, University of Aveiro, 3810-193 Aveiro, Portugal*

[d] *Department of Chemistry, CQ-VR, University of Trás-os-Montes e Alto Douro, 5001-801 Vila Real, Portugal*

Electronic Supporting Information

To whom correspondence should be addressed:

Filipe A. Almeida Paz
Department of Chemistry, CICECO
University of Aveiro
3810-193 Aveiro
Portugal

E-mail: filipe.paz@ua.pt
FAX: (+351) 234 401470
Telephone: (+351) 234 370200 (Ext. 23553)

Table of Contents

1. Characterization of the organic molecules

1.1. 2-Chloro-4,6-bis(methoxycarbonylmethylamine)-1,3,5-triazine (*L'*)

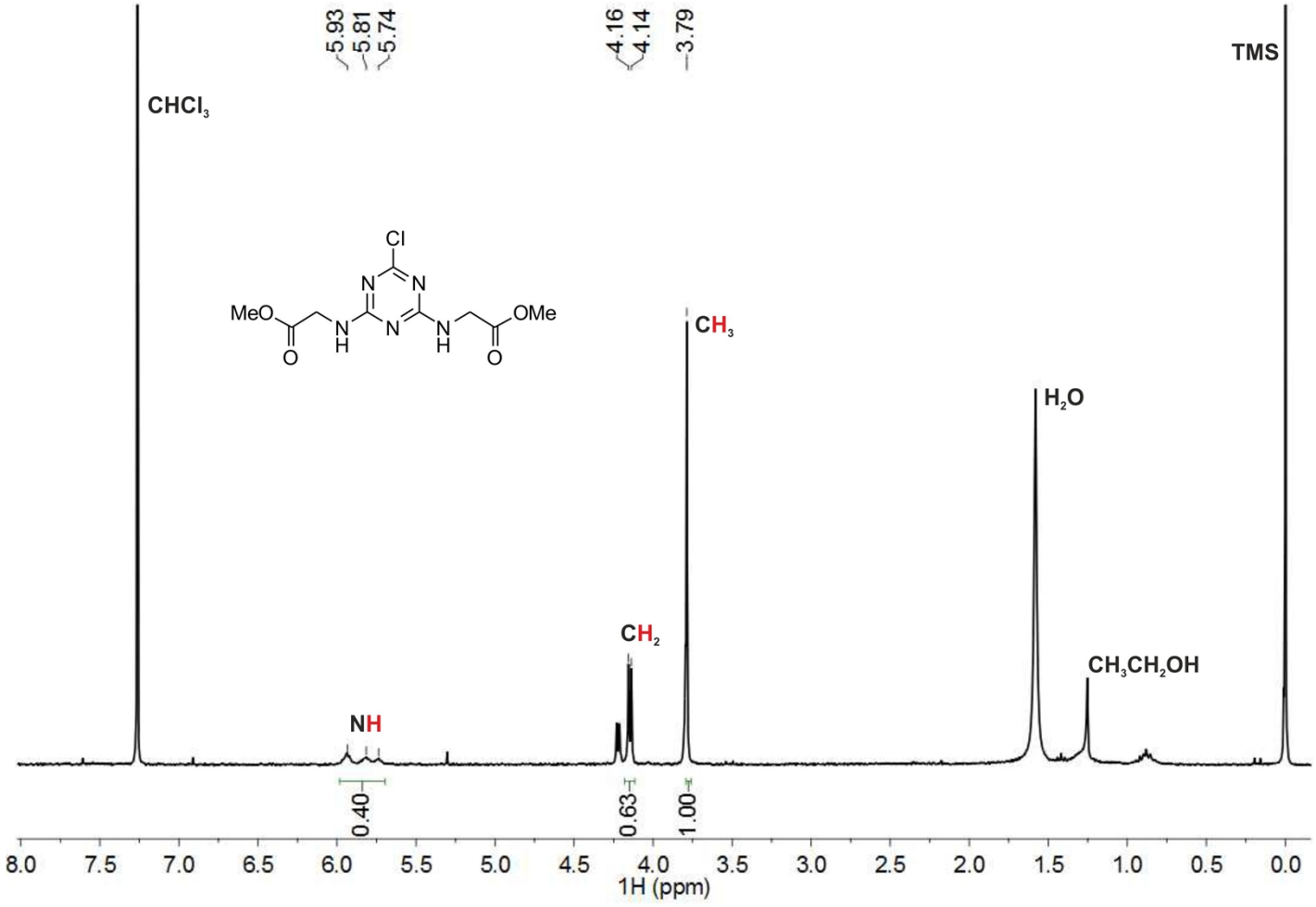

Fig. S1 ^{1}H NMR spectrum of 2-chloro-4,6-bis(methoxycarbonylmethylamine)-1,3,5-triazine in $CDCl_3$.

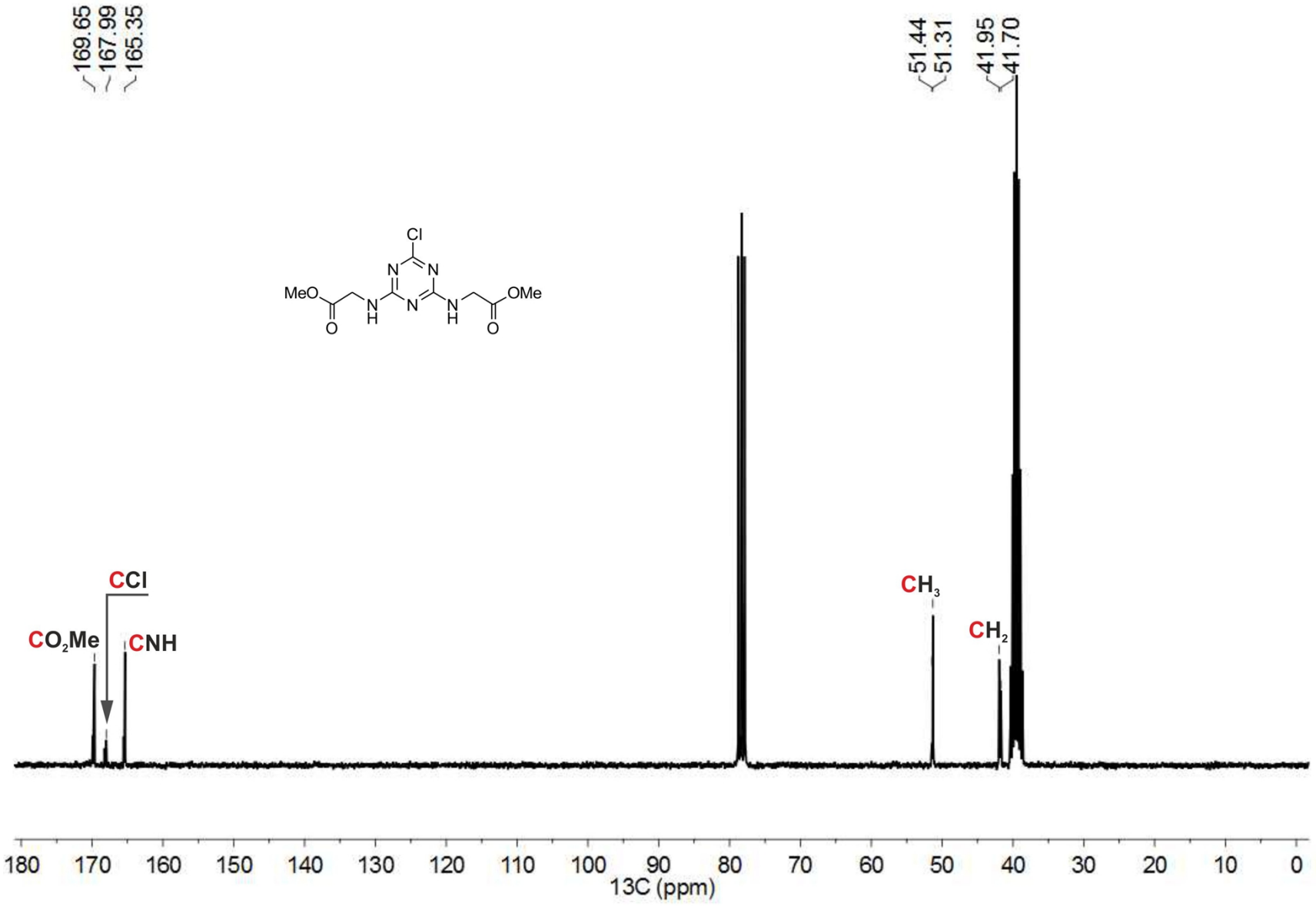

Fig. S2 ^{13}C NMR spectrum of 2-chloro-4,6-bis(methoxycarbonylmethylamine)-1,3,5-triazine in $CDCl_3$.

Mass Spectrometry

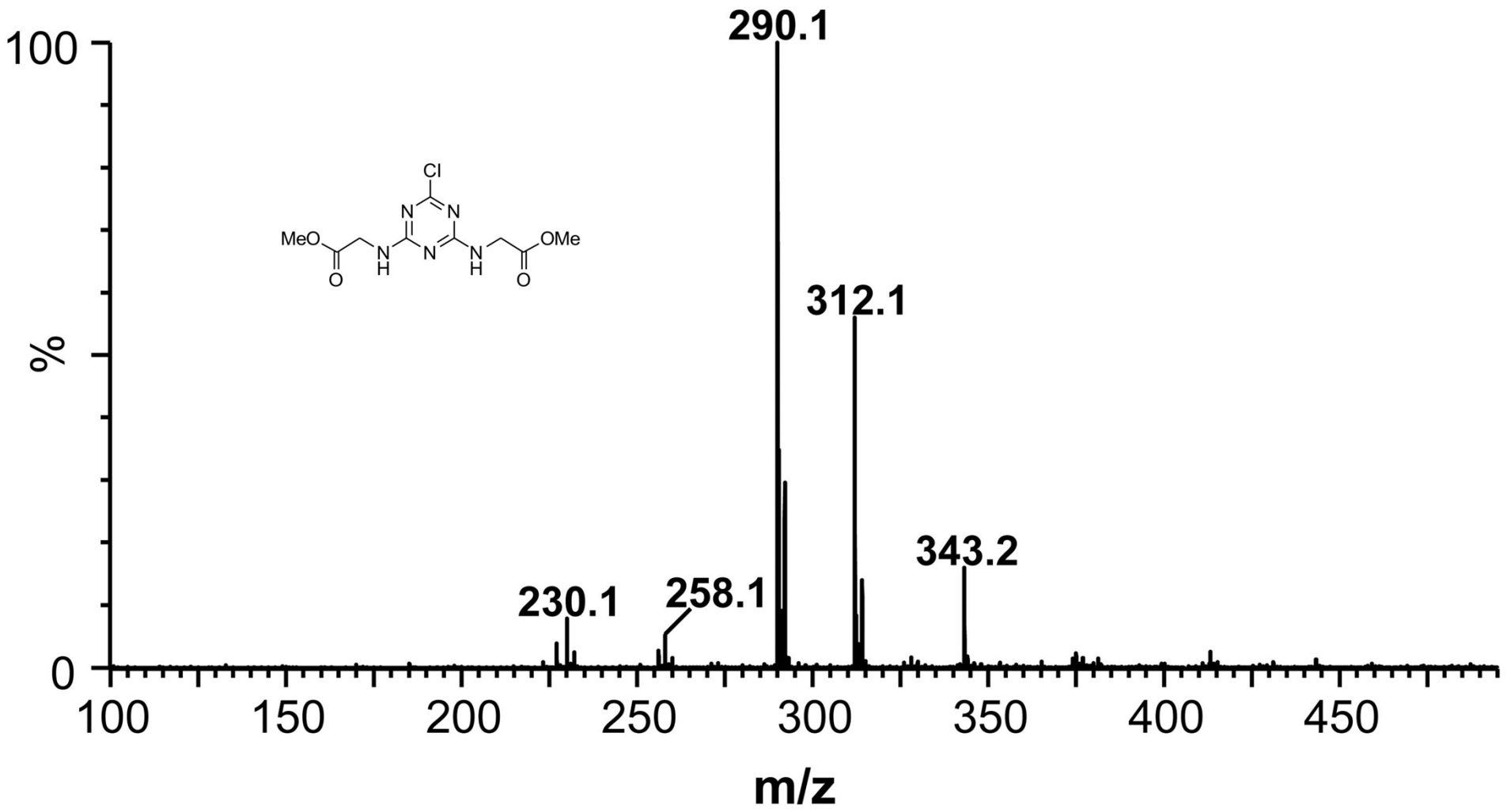

Fig. S3 Mass spectrum of 2-chloro-4,6-bis(methoxycarbonylmethylamine)-1,3,5-triazine.

1.2. 4,6-Bis(carboxymethylamino)-2-oxo-2,3-dihydro-1,3,5-triazin-1-ium chloride (H_2bodt·HCl)

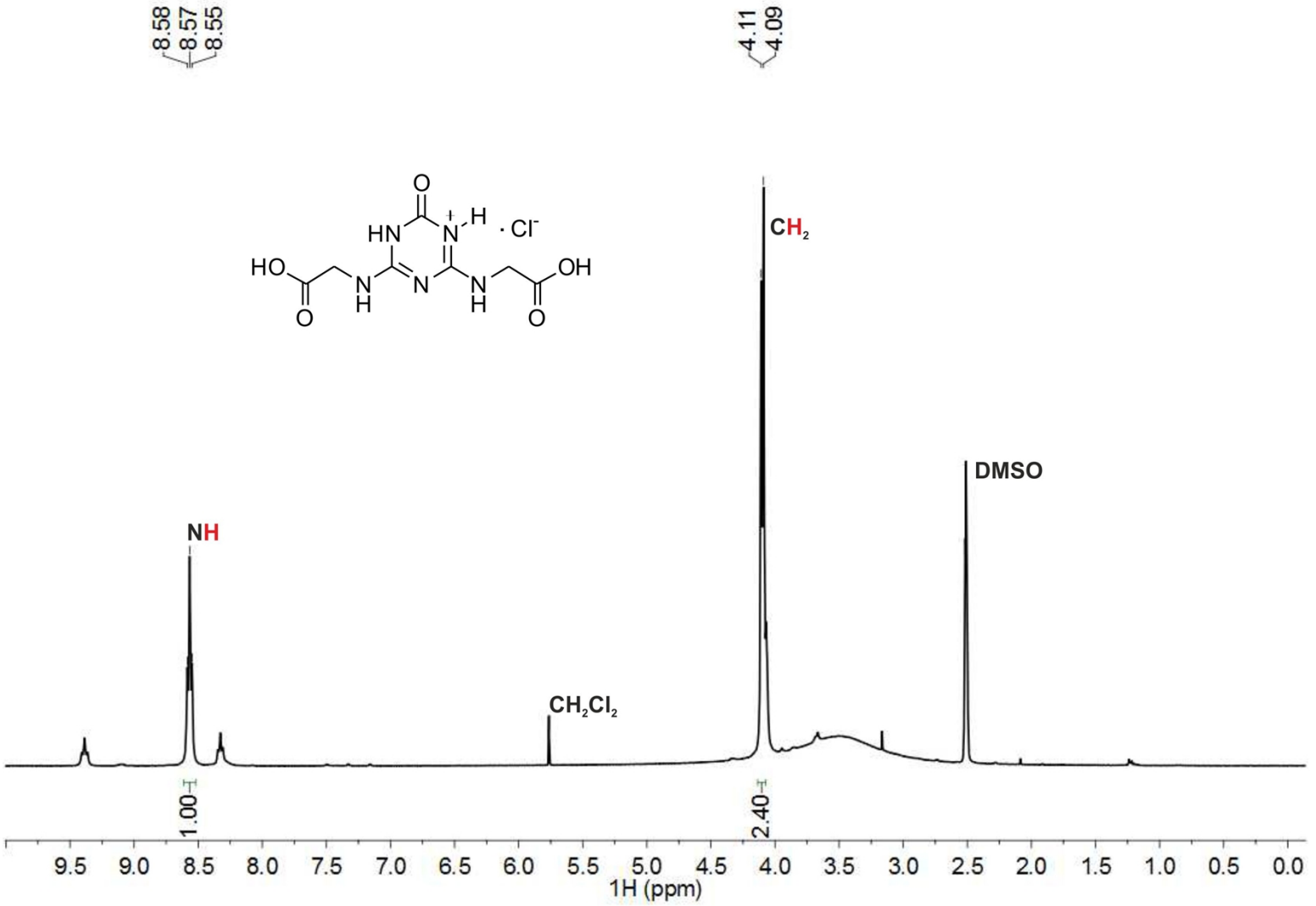

Fig. S4 ^{1}H NMR spectrum of 4,6-bis(carboxymethylamino)-2-oxo-2,3-dihydro-1,3,5-triazin-1-ium chloride in DMSO-d_6.

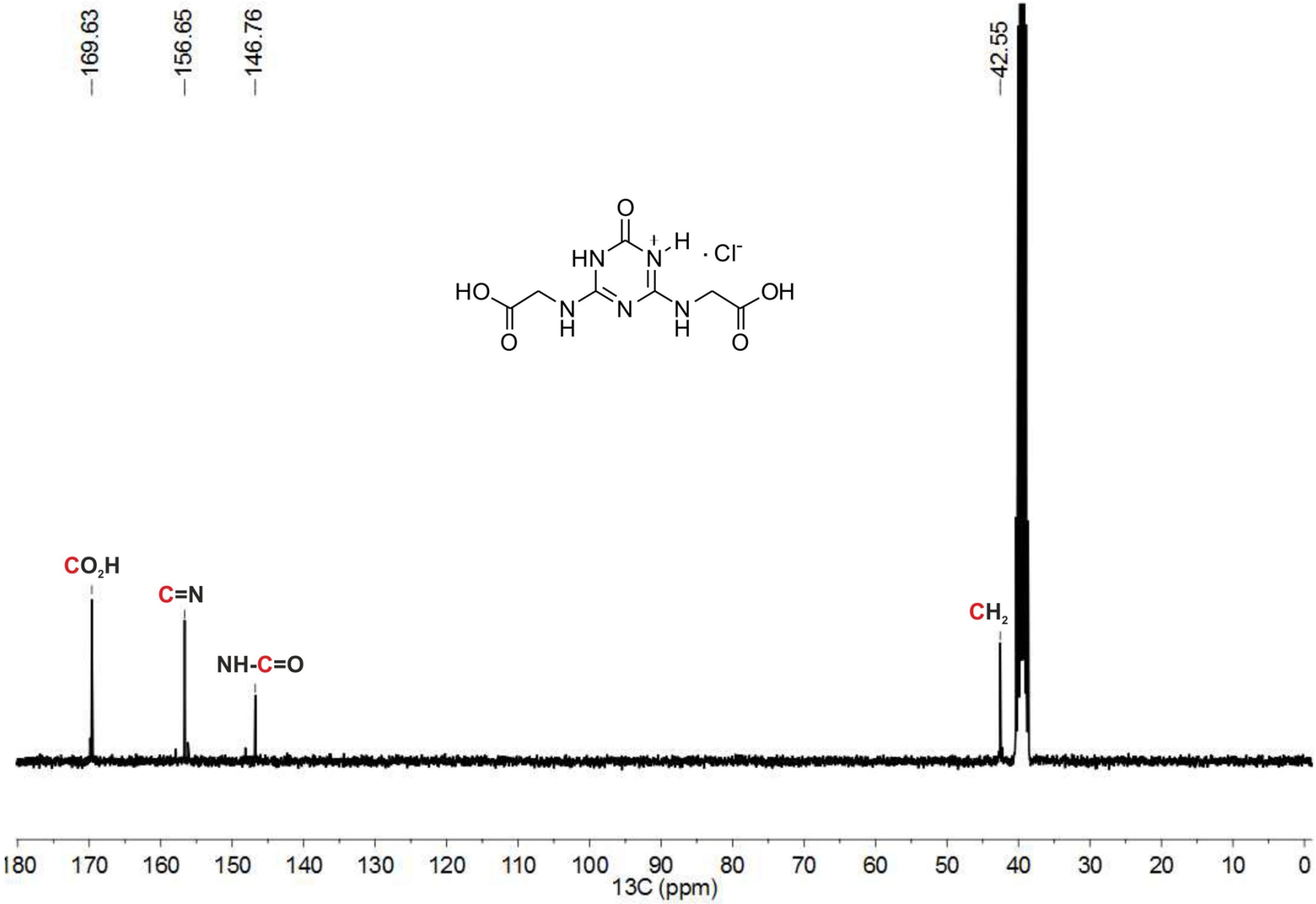

Fig. S5 ^{13}C NMR spectrum of 4,6-bis(carboxymethylamino)-2-oxo-2,3-dihydro-1,3,5-triazin-1-ium chloride in DMSO-d_6.

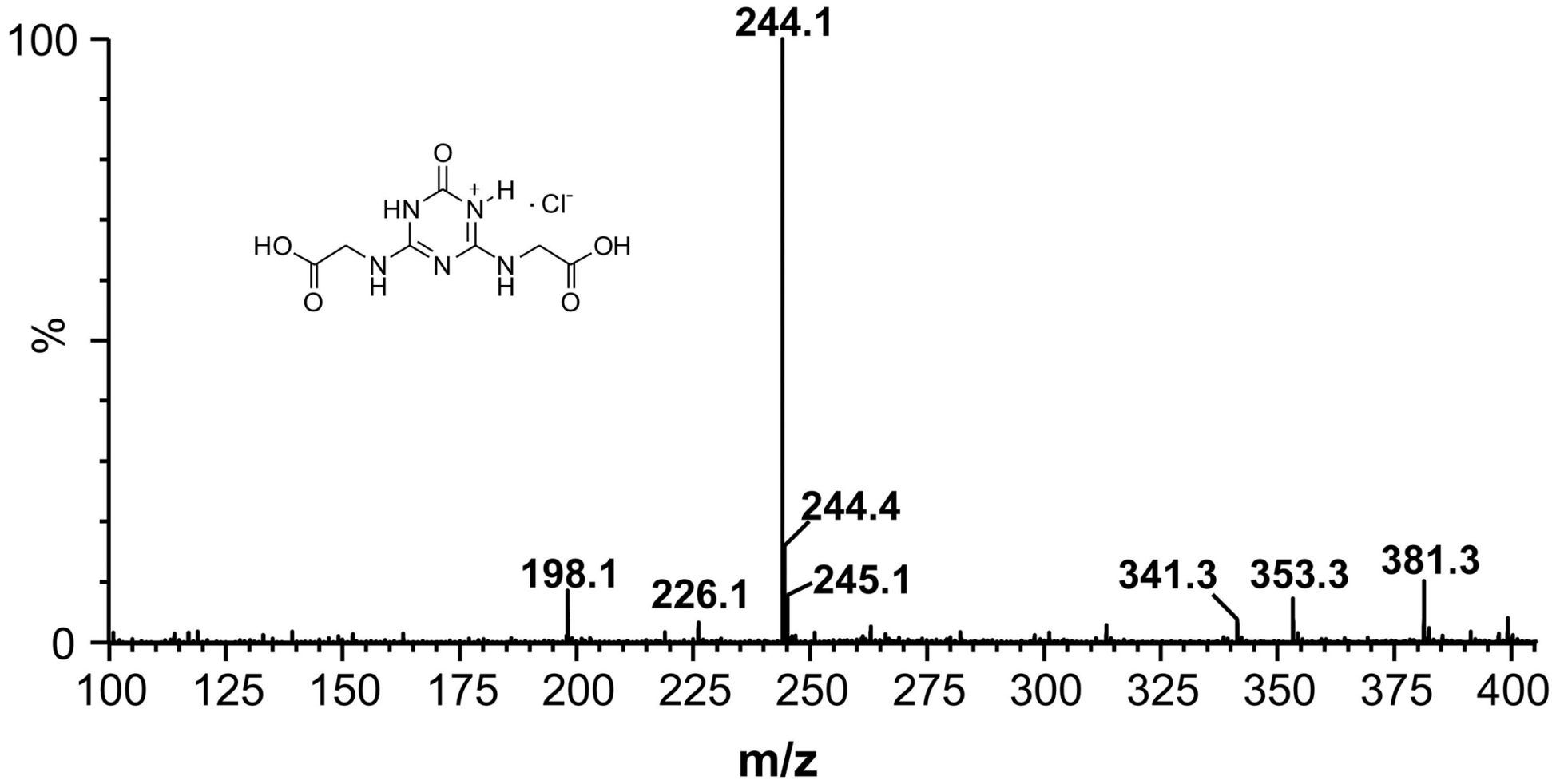

Fig. S6 Mass spectrum of 4,6-bis(carboxymethylamino)-2-oxo-2,3-dihydro-1,3,5-triazin-1-ium chloride.

2. Electron microscopy studies: EDS mapping

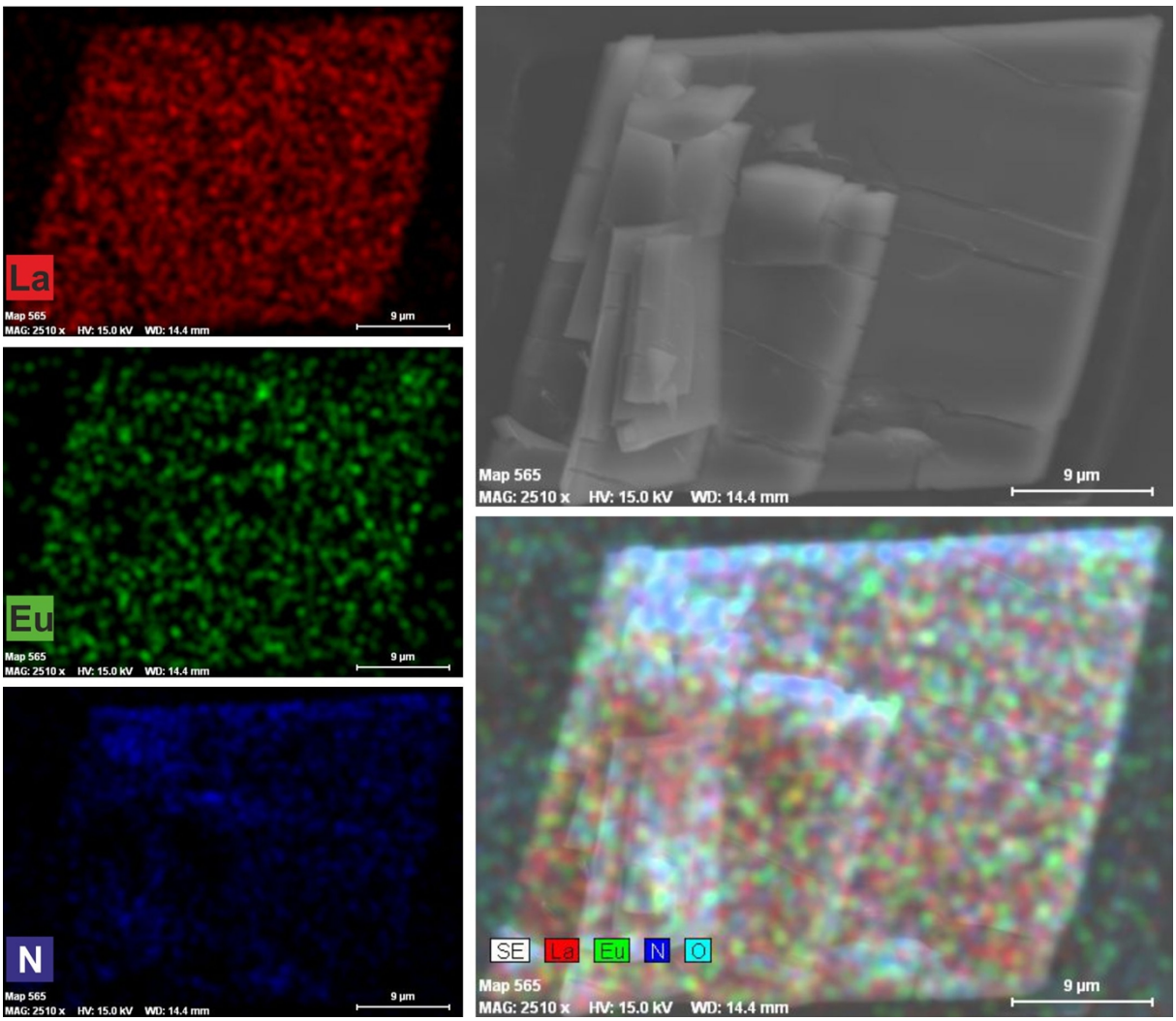

Fig. S7 Electron microscopy EDS mapping studies of a portion of the bulk $[(La_{0.95}Eu_{0.05})(bodt)(Hbodt)]$ (**2**) material.

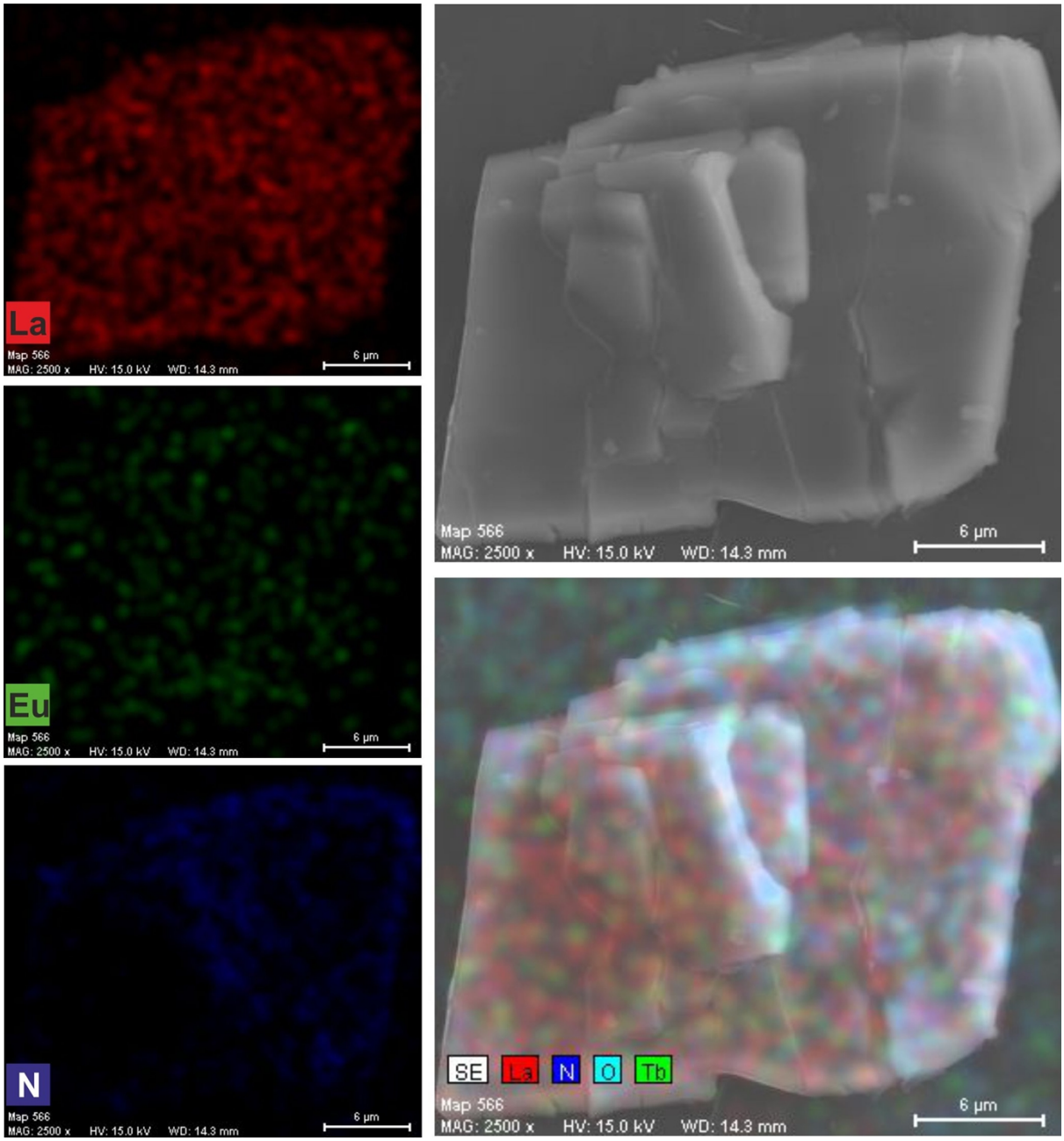

Fig. S8 Electron microscopy EDS mapping studies of a portion of the bulk $[(La_{0.95}Tb_{0.05})(bodt)(Hbodt)]$ (**3**) material.

3. Single-crystal X-ray diffraction studies

3.1. 2-Chloro-4,6-bis(methoxycarbonylmethylamine)-1,3,5-triazine (*L'*)

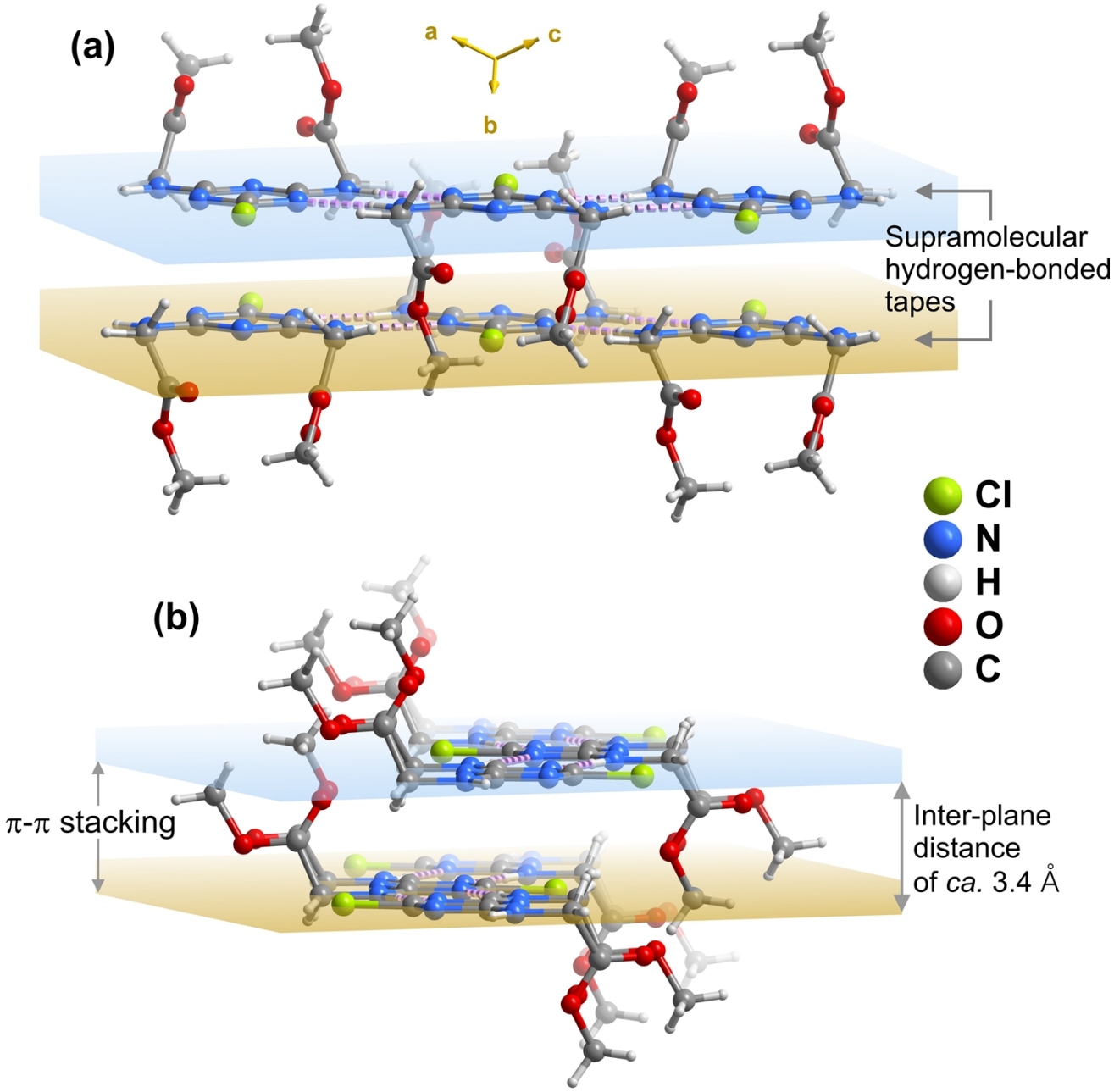

Fig. S9 Offset π-π interactions between neighbouring supramolecular tapes in the crystal structure of the intermediate compound ***L'***.

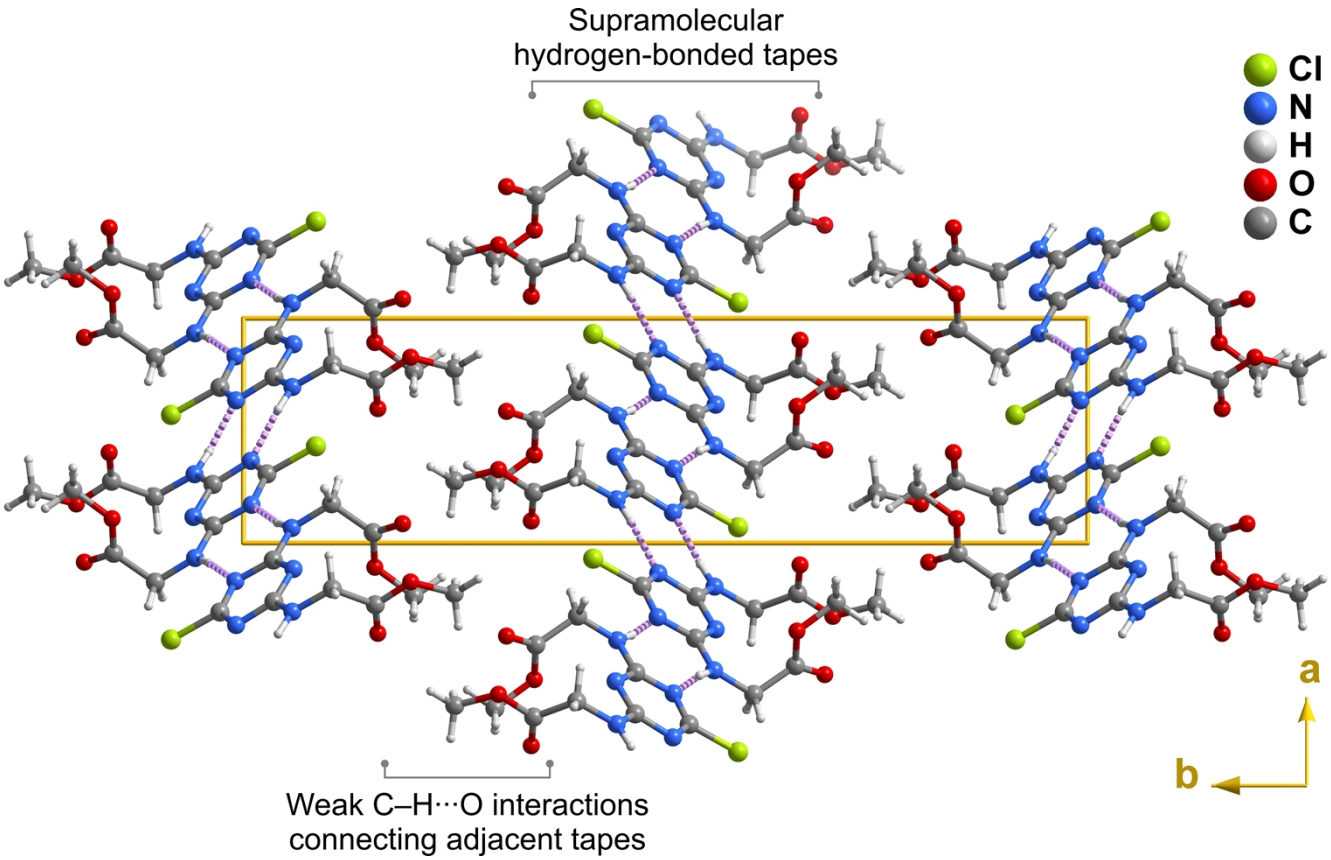

Fig. S10 Crystal packing of the intermediate compound ***L'*** viewed in perspective along the [001] direction of the unit cell. N–H··N hydrogen bonds are represented as dashed purple lines. For hydrogen bonding geometrical details see Table 2 (in the main paper).

3.2. 4,6-bis(carboxymethylamino)-2-oxo-2,3-dihydro-1,3,5-triazin-1-ium chloride (H_2bodt·HCl)

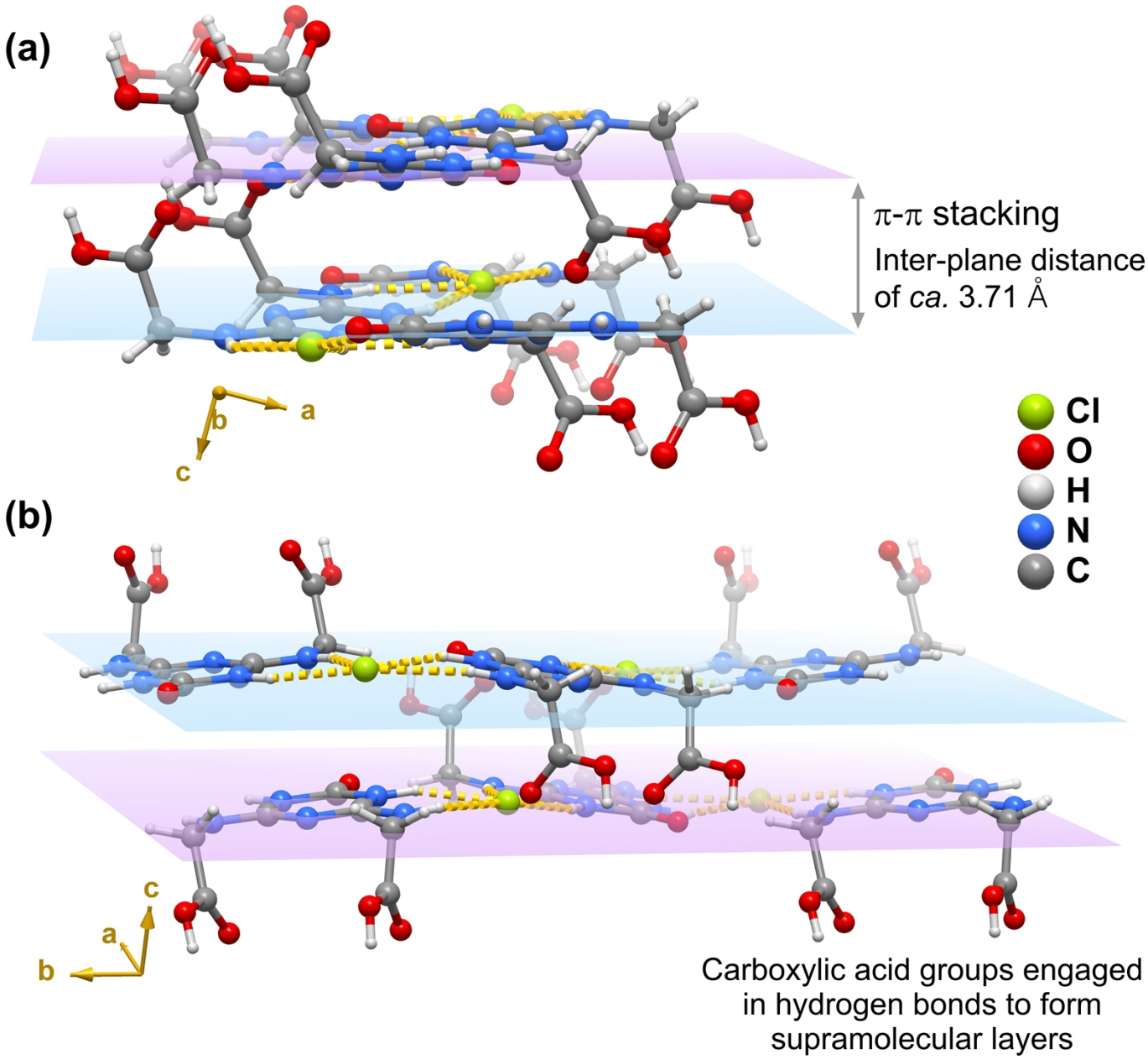

Fig. S11 Offset π-π interactions between neighbouring supramolecular tapes running along the [010] direction of the unit cell in the crystal structure of the supramolecular salt H_2bodt·HCl.

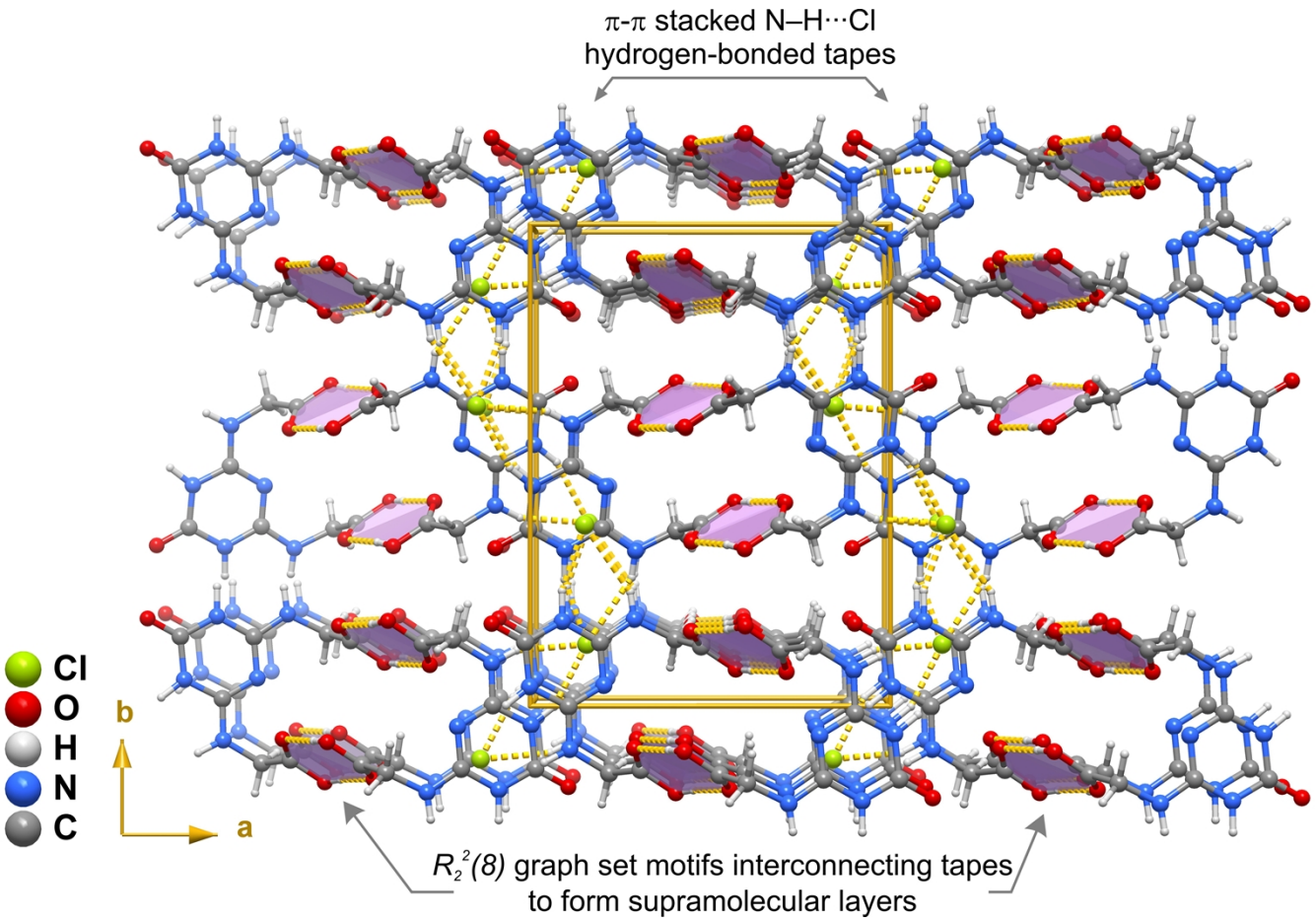

Fig. S12 Crystal packing of the supramolecular salt H_2bodt·HCl viewed in perspective along the [001] direction of the unit cell. O–H···O and N–H···Cl hydrogen bonds are represented as dashed orange lines. For hydrogen bonding geometrical details see Table 3 (in the main paper).

3.3. Coordination polymer [La(bodt)(Hbodt)] (1)

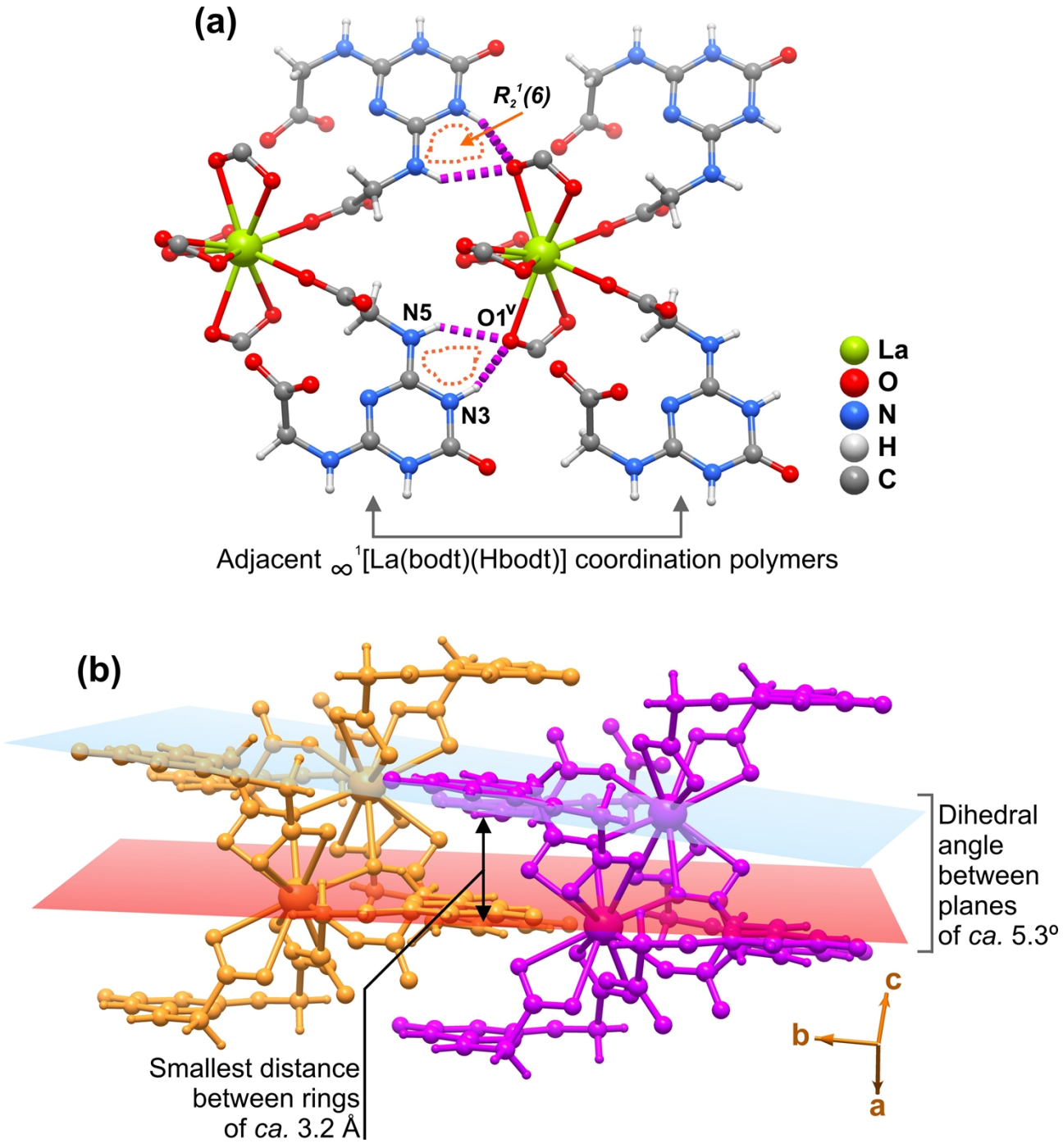

Fig. S13 Supramolecular contacts between spatially-close $_\infty^1$[La(bodt)(Hbodt)] coordination polymers belonging to different supramolecular 3D networks. **(a)** Bifurcated N–H···O hydrogen bonding interactions forming a $\mathbf{R}_2^1(6)$ graph set motif. **(b)** Offset contacts between rings belonging to the organic ligands. For hydrogen bonding geometric details see Table 5 (in the main paper). Symmetry transformation used to generate equivalent atoms: (v) *x*, *1-y*, *½+z*.

4. Thermogravimetry

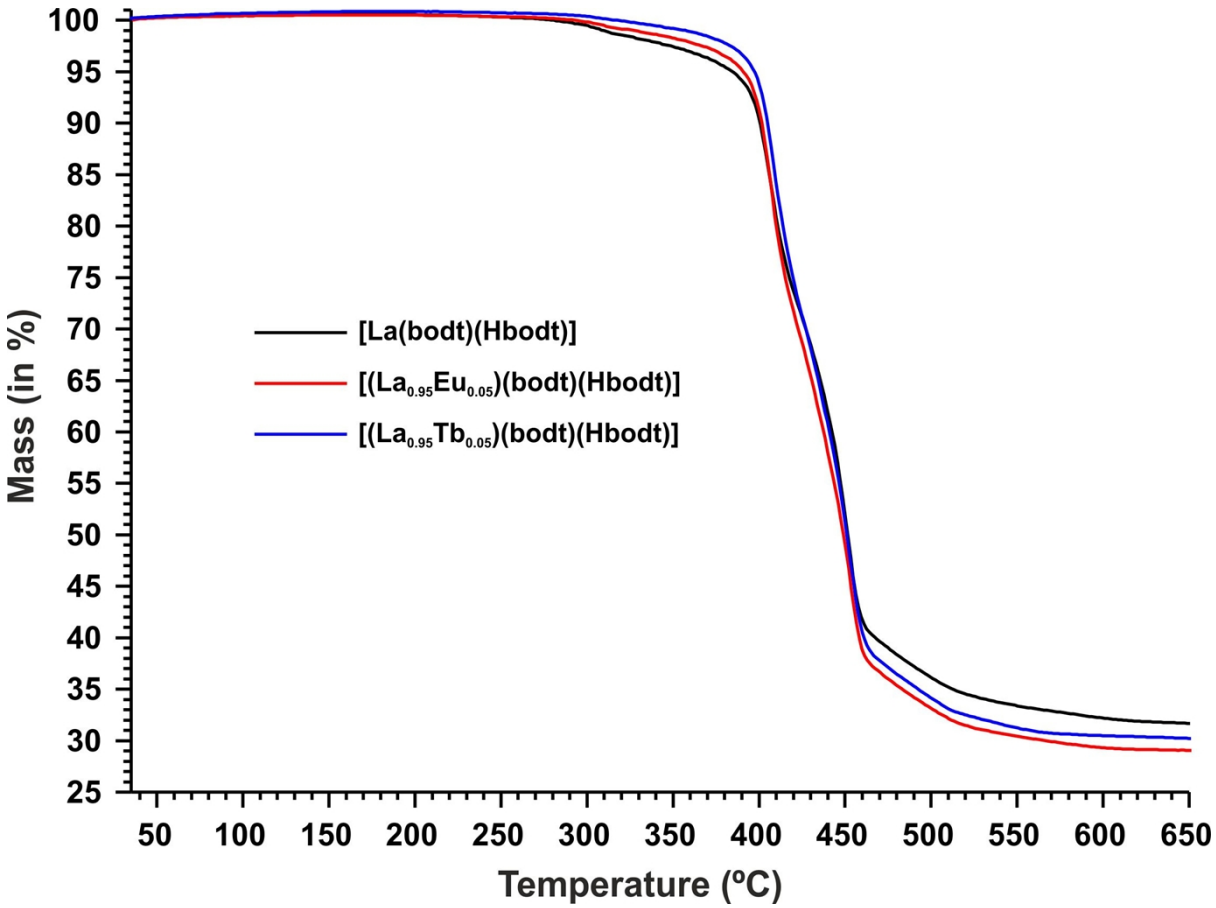

Fig. S14 Thermogravimetric curves of the [Ln(bodt)(Hbodt)] materials [where Ln^{3+} = La^{3+} (**1**), $(La_{0.95}Eu_{0.05})^{3+}$ (**2**) and $(La_{0.95}Tb_{0.05})^{3+}$ (**3**)].

5. FT-IR spectroscopy

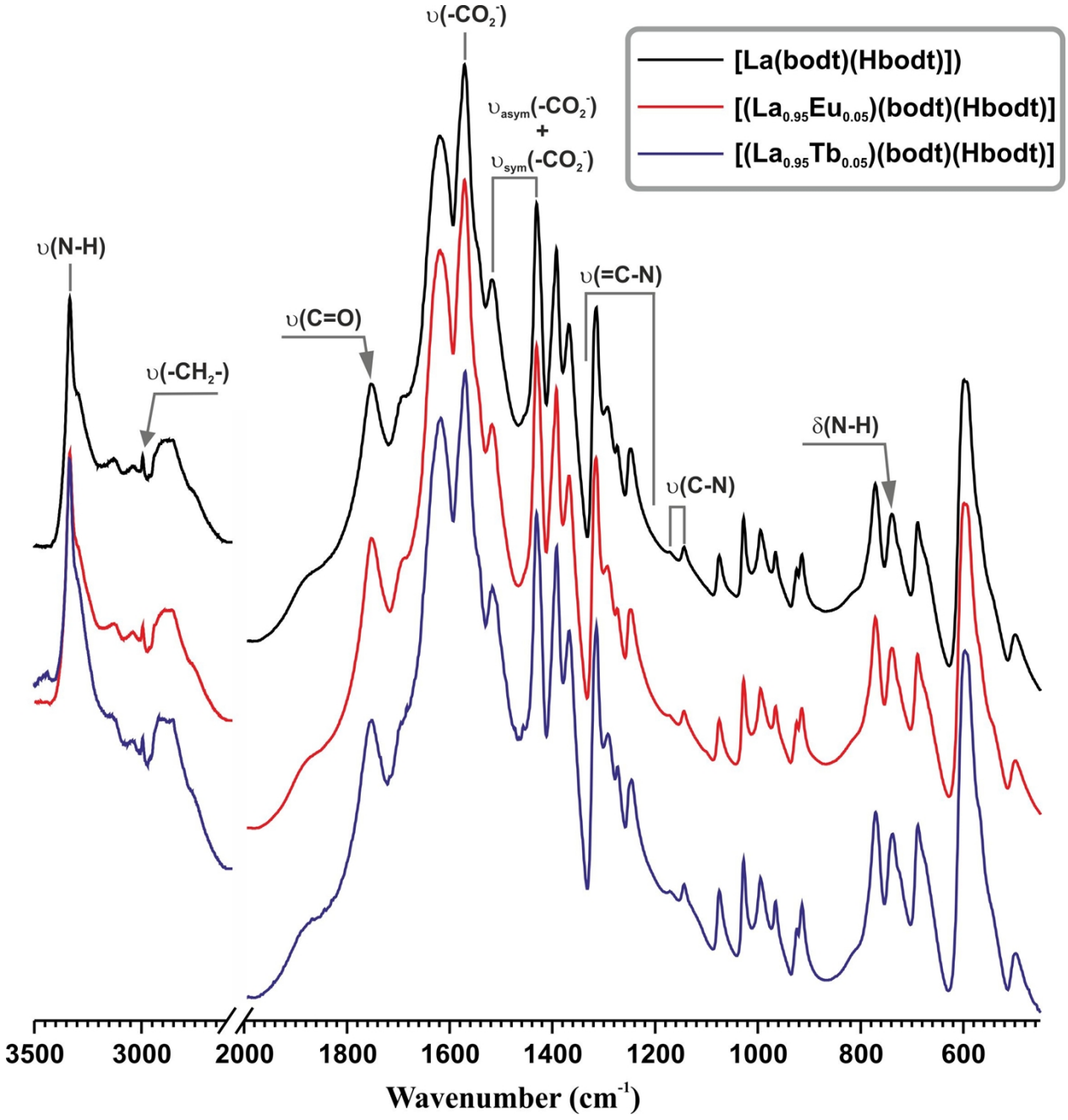

Fig. S15 FT-IR spectra of [Ln(bodt)(Hbodt)] materials [where Ln^{3+} = La^{3+} (**1**), $(La_{0.95}Eu_{0.05})^{3+}$ (**2**) and $(La_{0.95}Tb_{0.05})^{3+}$ (**3**)].

6. Photoluminescence spectroscopy and TD-DFT calculations

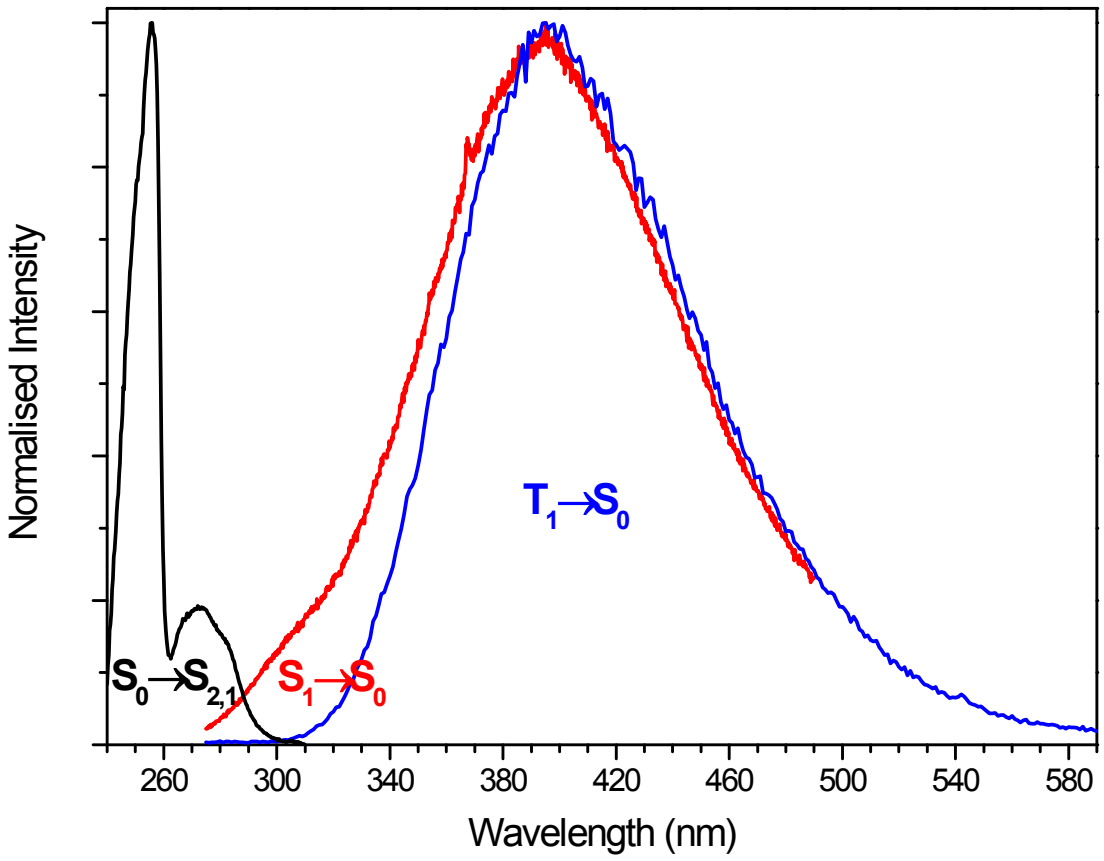

Fig. S16 Stationary state excitation (black line; $\lambda_{Em.}$= 420 nm) and emission (red line; $\lambda_{Exc.}$ = 255 nm) spectra of [La(bodt)(Hbodt)] (**1**) collected at 12 K. The time-resolved emission spectrum (blue line; $\lambda_{Exc.}$ = 255 nm; initial delay of 0.5 ms and integration time of 10 ms) is provided for comparative purposes. Emission spectra were not corrected for the instrument response.

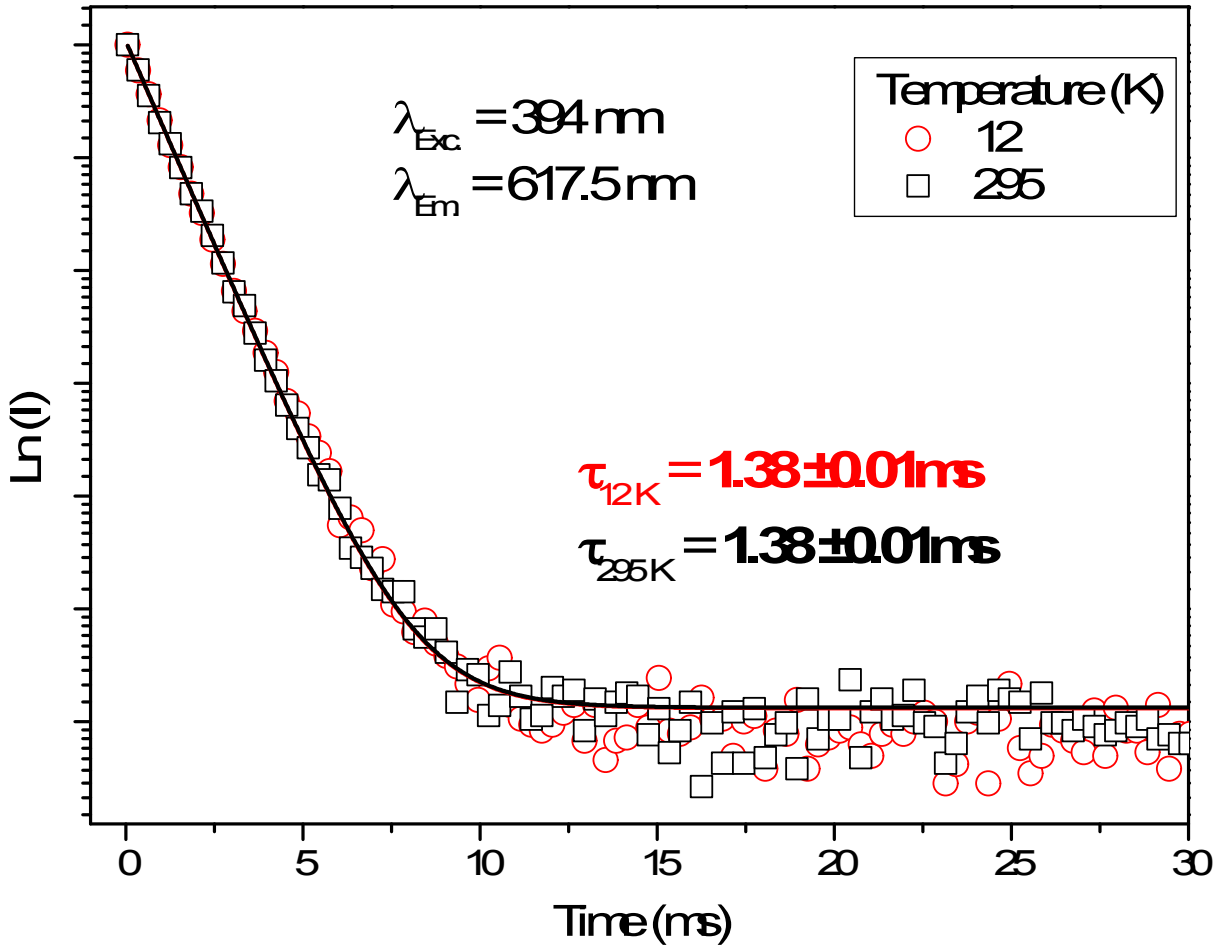

Fig. S17 $^5D_0$ decay curves of the [$(La_{0.95}Eu_{0.05})$(bodt)(Hbodt)] (**2**) material and the corresponding fitting lines.

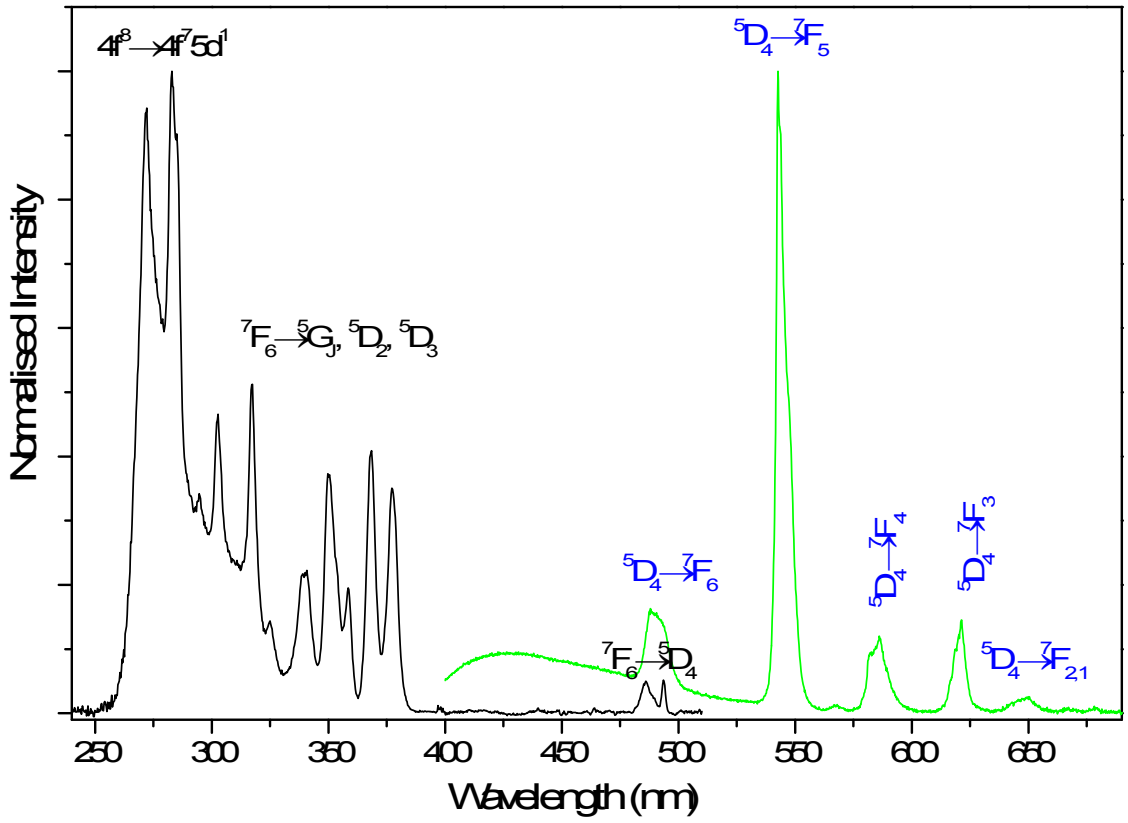

Fig. S18 Ambient temperature excitation and emission spectra of the $[(La_{0.95}Tb_{0.05})(bodt)(Hbodt)]$ (**3**) material. The emission was detected at 543 nm and the excitation was fixed at 283 nm.

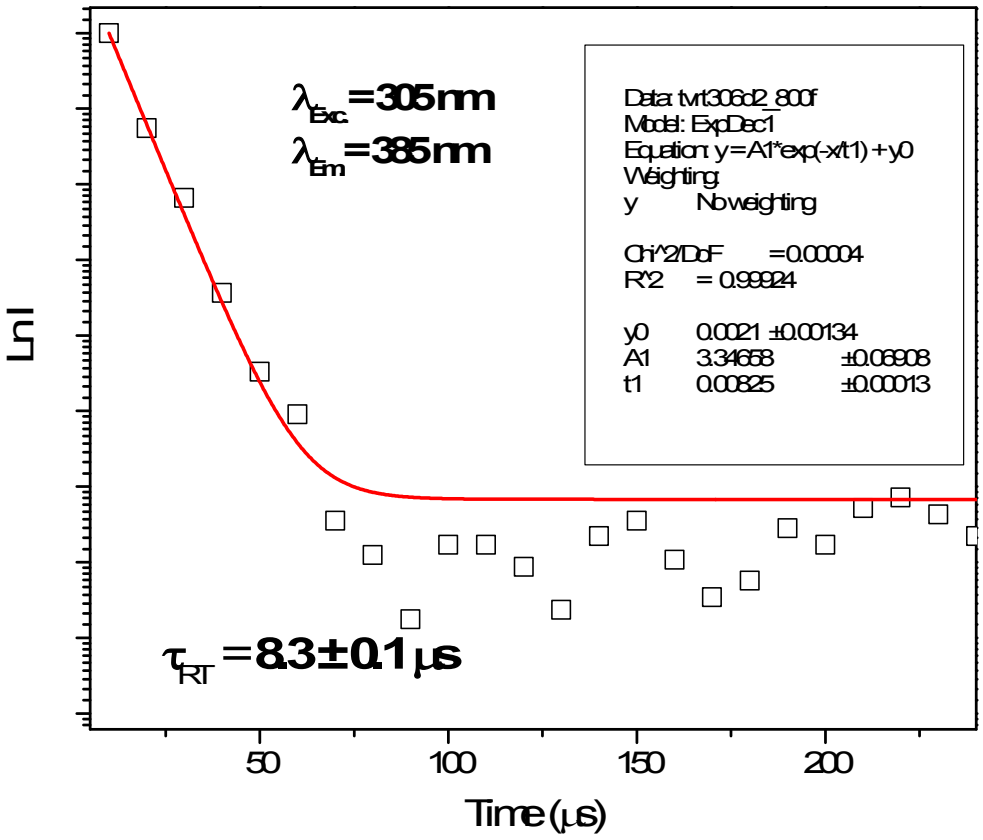

Fig. S19 Ambient temperature decay curve and the corresponding single exponential decay fitting line of the proton transfer emission of [La(bodt)(Hbodt)] (**1**) detected at 385 nm with excitation at 305 nm. Each decay point corresponds to the average intensity obtained from 800 lamp flash excitation. *Please note*: because the employed phosphorometer could not discriminate time values lower than 10 μs, the fitted value and the corresponding error (calculated from the fit) should be considered as a rough estimation of the emission lifetime.

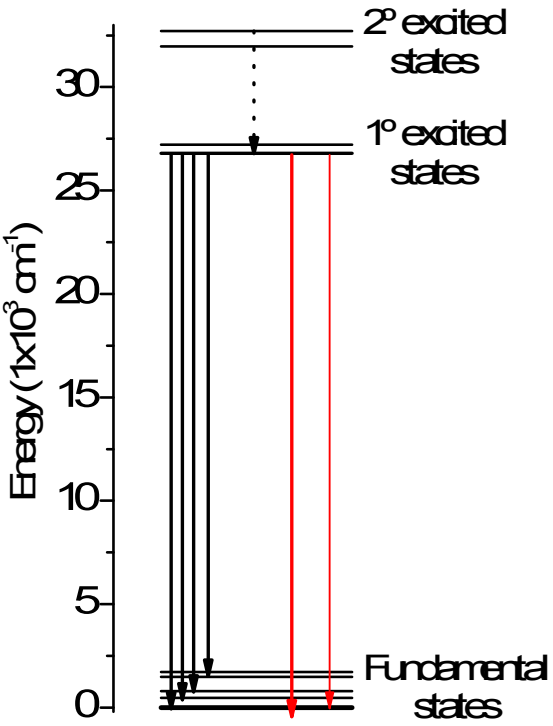

Fig. S20 Tentative energy scheme demonstrating the emission process in [La(bodt)(Hbodt)] (**1**) at ambient temperature (black arrows) and at 12 K (red arrows). The solid arrows denote radiative emission and the dotted one denotes non-radiative relaxation.

Table S1 Partial molecular orbital compositions in the ground-state singlet (S_0) for the simplified model. H and L correspond to the highest occupied and the lowest unoccupied molecular orbitals, respectively.

Orbital	Carboxymethylamino group	Triazine -derivative ring	La
H-5	31.26	66.68	2.06
H-4	29.64	69.09	1.27
H-3	43.31	55.91	0.77
H-2	38.66	59.26	2.08
H-1	42.44	54.18	3.38
H	55.34	42.82	1.84
L	51.04	5.93	43.03
L+1	47.06	1.44	51.50
L+2	58.02	4.44	37.54
L+3	25.71	4.90	69.39

Table S2 Partial molecular orbital compositions in the lowest-lying singlet excited state (S_1) for the simplified model. H and L correspond to the highest occupied and the lowest unoccupied molecular orbitals, respectively.

Orbital	Carboxymethylamino group	Triazine -derivative ring	La
H-6	29.44	69.67	0.90
H-5	18.35	81.57	0.08
H-4	42.60	55.03	2.37
H-3	37.82	62.08	0.10
H-2	32.48	66.84	0.68
H-1	43.25	53.62	3.13
H	49.98	48.32	1.71
L	24.79	75.06	0.15

Table S3 Calculated TD-B3LYP excitations in the ground-state singlet (S_0) for the simplified model.

λ(nm)[a]	f[b]	Composition[c]	CI[d]
315	0.0048	H-1 → L+2	0.12897
		H → L+2	0.64387
		H → L+3	0.24661
283	0.0067	H-5 → L	0.42814
		H-4 → L	0.33618
		H-2 → L	0.36102

[a] Only selected excited states are presented.
[b] Oscillator strength.
[c] Only the three primary transitions are reported; H stands for HOMO and L stands for LUMO.
[d] The CI coefficients are in absolute values.

Table S4 Calculated TD-B3LYP de-excitations in the lowest-lying singlet excited state (S_1) for the simplified model.

λ(nm)[a]	f[b]	Composition[c]	CI[d]
454	0.0163	H-2 → L	0.64910
		H-1 → L	0.21405
332	0.0101	H-6 → L	0.46506
		H-4 → L	0.14264
		H-3 → L	0.46718

[a] Only selected excited states are presented.
[b] Oscillator strength.
[c] Only the three primary transitions are reported; H stands for HOMO and L stands for LUMO.
[d] The CI coefficients are in absolute values.